Empirical instability strip for classical Cepheids. I. The Large Magellanic Cloud galaxy

F. Espinoza-Arancibia, B. Pilecki, G. Pietrzyński, R. Smolec, P. Kervella

A&A, 682, A185 (2024)
https://doi.org/10.1051/0004-6361/202347804

Astronomy & Astrophysics

Empirical instability strip for classical Cepheids

I. The Large Magellanic Cloud galaxy

F. Espinoza-Arancibia[1], B. Pilecki[1], G. Pietrzyński[1], R. Smolec[1], and P. Kervella[2]

[1] Nicolaus Copernicus Astronomical Center, Polish Academy of Sciences, Bartycka 18, 00-716 Warsaw, Poland
e-mail: fespinoza@camk.edu.pl
[2] LESIA (UMR 8109), Observatoire de Paris, PSL, CNRS, UPMC, Univ. Paris-Diderot, 5 place Jules Janssen, 92195 Meudon, France

Received 25 August 2023 / Accepted 24 November 2023

ABSTRACT

Context. The instability strip (IS) of classical Cepheids has been extensively studied theoretically. Comparing the theoretical IS edges with those obtained empirically, using the most recent Cepheids catalogs available, can provide us with insights into the physical processes that determine the position of the IS boundaries.
Aims. We aim to investigate the empirical positions of the IS of the classical Cepheids in the Large Magellanic Cloud (LMC), considering any effect that increases its width, to obtain intrinsic edges that can be compared with theoretical models.
Methods. We used data of classical fundamental-mode (F) and first-overtone (1O) LMC Cepheids from the OGLE-IV variable star catalog, together with a recent high-resolution reddening map from the literature. Our final sample includes 2058 F and 1387 1O Cepheids. We studied their position on the Hertzsprung-Russell diagram and determined the IS borders by tracing the edges of the color distribution along the strip.
Results. We obtained the blue and red edges of the IS in V- and I-photometric bands, in addition to $\log T_{\rm eff}$ and $\log L$. The results obtained show a break located at the Cepheids' period of about three days, which was not reported before. We compared our empirical borders with theoretical ones published in the literature, obtaining a good agreement for specific parameter sets.
Conclusions. The break in the IS borders is most likely explained by the depopulation of second- and third-crossing classical Cepheids in the faint part of the IS, since blue loops of evolutionary tracks in this mass range do not extend blueward enough to cross the IS at the LMC metallicity. Results from the comparison of our empirical borders with theoretical ones prove that our empirical IS is a useful tool for constraining theoretical models.

Key words. stars: evolution – stars: variables: Cepheids – Magellanic Clouds

1. Introduction

During their evolution, intermediate- and high-mass stars can radially pulsate as classical Cepheids (hereafter Cepheids) when they cross a defined region in the Hertzsprung-Russel diagram (HRD), called the instability strip (IS). Cepheids span a typical mass range between 3 and 13 $M_\odot$ (see, e.g., Bono et al. 2000a; Anderson et al. 2016), though Cepheids with masses higher than 13 $M_\odot$ have also been identified (Musella 2022 and references therein). With the exception of the most massive Cepheids, such stars first cross the IS during the H-shell burning phase, after they leave the main sequence (MS)[1]. Later, the star crosses the IS again during the He-core burning phase, which is called the blue loop. The timescale of the first crossing is about 100 times shorter than that of subsequent crossings. Thus, it is assumed that most of the observed Cepheids are burning He during the second or third crossing of the IS.

The location of the blue edge of the IS is related to the location of the partial ionization layers. These crucial zones, responsible for the excitation of radial pulsation by the so-called κ and γ mechanisms, could either be located too far out or not be present at all if the star is sufficiently hot (see, e.g., Catelan & Smith 2015 and references therein). At the red end, convection produces a stabilizing effect that eventually quenches pulsation. Therefore, the exact location of the red edges depends on the complex interplay between pulsation and convection (see Houdek & Dupret 2015 for a review and references). Similarly, the IS has proven not to be a "strip", but rather to have a "wedge" structure. The structure of the IS was reported initially using Galactic Cepheids by Pel & Lub (1978) and Fernie (1990), while in the Magellanic Clouds, it was noted by Martin et al. (1979) and Caldwell & Laney (1991). A large number of theoretical studies have addressed the effects on the IS structure due to different physical properties. Among them, Bono et al. (2000b) showed how nonlinear theoretical models that consider the coupling between pulsation and convection produce an IS much less steep than linear models. Fiorentino et al. (2002), and more recently De Somma et al. (2022), concluded that the IS location depends on both the metallicity and He abundance, moving to lower effective temperatures as the metal content increases or the He abundance decreases. Petroni et al. (2003) studied the effect of using different equations of state on the IS topology, finding a weak dependence. Fiorentino et al. (2007) explored the effects of varying the mixing-length parameter $l/H_{\rm P}$, finding that the IS becomes narrower as $l/H_{\rm P}$ increases; these results agree with the recent work done by De Somma et al. (2022).

[1] High-mass stars ($\gtrsim$9 $M_\odot$) start He-core burning on the way to the red giant branch (RGB) phase, during their first and only crossing of the IS (see, e.g., Anderson et al. 2016).

Anderson et al. (2016) conducted a study of the effects of rotation on Cepheid models, finding that the blue edge of the IS does not depend significantly on rotation, while the red edge is affected by metallicity and rotation.

On the other hand, empirical studies have been conducted to study the properties of the IS. Turner (2001) mapped the IS with a sample of 293 Cepheids in the Milky Way with reddening measurements, finding agreement with the results of Pel & Lub (1978), but disagreement with those presented by Fernie (1990). Tammann et al. (2003) obtained period-color and period-luminosity (P–L) relations of a sample of 321 Galactic Cepheids, in addition to 314 and 486 Cepheids from the Large Magellanic Cloud (LMC) and the Small Magellanic Cloud (SMC), respectively. Using these relations, they obtained the IS of the Galaxy and the Magellanic Clouds, finding differences in the slopes of the ISs between the three galaxies. Sandage et al. (2004, 2009) presented a detailed analysis of the samples of 593 and 460 Cepheids from the LMC and SMC, respectively. For both, they found breaks in the P–L relations, as well as in the IS edges, located at Cepheids' periods of ten days (for the LMC) and 2.5 days (for the SMC). Recently, to find candidates for non-pulsating stars lying inside the IS, Narloch et al. (2019) determined a simple empirical instability strip for a sample of over 3200 LMC Cepheids. They used a step-detection technique and obtained almost parallel edges without a break. However, these authors did not take measures to clean the sample of outliers, and they did not further analyze the obtained IS.

Remarkably, the Optical Gravitational Lensing Experiment (OGLE) project presented an almost complete census of Cepheids in the Magellanic Clouds (Soszyński et al. 2017). In addition, numerous reddening maps have been published in the literature (see, e.g., Inno et al. 2016; Górski et al. 2020; Skowron et al. 2021; Chen et al. 2022). In this context, we aim to obtain an empirical intrinsic IS for the Cepheids in the LMC using the most recent Cepheids catalogs available. The comparison of theoretical IS edges with those obtained empirically can provide insights into the physical processes that determine the position of the IS boundaries. For this purpose, we used data of classical fundamental-mode (F) and first-overtone (1O) LMC Cepheids from the OGLE variable star catalog, together with recent high-resolution reddening maps from the literature. We studied the position of the Cepheids on the color-magnitude diagram (CMD) and determined the IS borders by tracing their color distribution along the strip. In addition, we compared our empirical borders with theoretical ones presented in the literature.

The outline of this paper is as follows. Section 2 describes the sample selection procedure; Sect. 3 describes the method used to obtain the IS borders; and Sect. 4 presents a discussion of our results, including a comparison with LMC eclipsing binary stars and theoretical ISs published in the literature. Finally, Sect. 5 presents our conclusions.

2. Sample selection

We used data of F and 1O Cepheids in the LMC from the OGLE-IV variable stars catalog (Soszyński et al. 2017) and OGLE-III Shallow Survey (Ulaczyk et al. 2013). The distribution in the CMD of the full sample consisting of 2335 F Cepheids and 1682 1O Cepheids is shown in Fig. 1.

The data are affected by reddening, produced by the interstellar extinction along the line of sight. To correct for this effect we used the high-resolution (1.7 arcmin × 1.7 arcmin) reddening map of Skowron et al. (2021), which is based on red clump stars

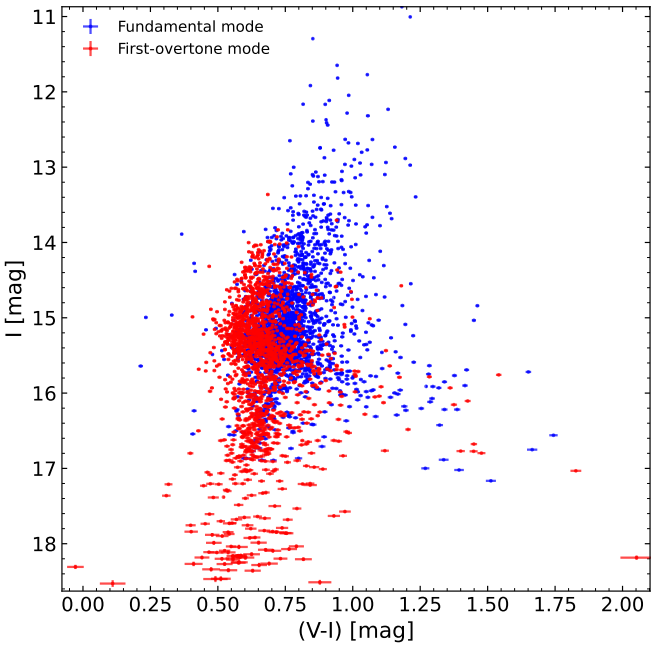

Fig. 1. Color-magnitude diagram of fundamental (blue) and first-overtone (red) LMC Cepheids from the OGLE-IV variable stars catalog.

from the Magellanic Clouds, selected from the OGLE-IV catalog. This map has shown good agreement with previous and other recent reddening maps (e.g., Inno et al. 2016; Chen et al. 2022), and yields a small dispersion compared to other maps in the literature. It also covers both the central part and the outskirts of the LMC. These features are important when trying to recover the intrinsic IS, as discussed in Sect. 3. We used the coefficients of relative extinction provided by Schlegel et al. (1998) to calculate the reddening correction.

In order to clean our sample, we discarded 164 objects deviating more than three sigma from the reddening-free period-luminosity relationship (also known as period-Wesenheit or P–W relation), as shown in Fig. 2. A significant fraction of them are objects located significantly above the P–L relationship, which were recently identified to be mostly binary Cepheids with giant companions (Pilecki et al. 2021, 2022; Pilecki 2022). Moreover, we discarded 112 Cepheids that presented remarks in the OGLE-IV catalog, to avoid objects that have uncertain characterization. In addition, following the method described in Madore et al. (2017), 113 Cepheids were not considered due to their high vertical deviation from the relation between the magnitude residuals of the I-band P–L relation and the corresponding residual of the P–W relation, as shown in Fig. 3. These deviations are possibly due to errors in the individual adopted extinctions (as mentioned by Madore et al. 2017). Since intrinsic color uncertainties are dominated by reddening uncertainties, as a final cleaning process, we did not consider Cepheids with reddening errors greater than the 95th percentile of the reddening error distribution. Consequently, 109 F Cepheids and 74 1O Cepheids were discarded.

Individual distances to the stars, used to calculate their I-band absolute magnitudes, were computed using the method described in Jacyszyn-Dobrzeniecka et al. (2016), which takes into account the geometry of the LMC. We adopted their P–L relations for the full sample of F and 1O LMC Cepheids but only those without a break. As for the LMC distance, we used

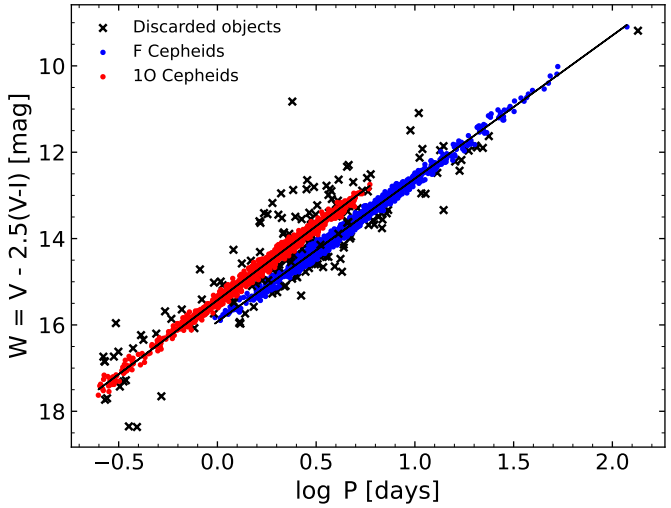

Fig. 2. Period-Wesenheit relations for fundamental (F, blue symbols) and first-overtone (1O, red symbols) LMC Cepheids. Discarded objects that deviate more than three sigma from the reddening-free P–L relation are marked with black crosses.

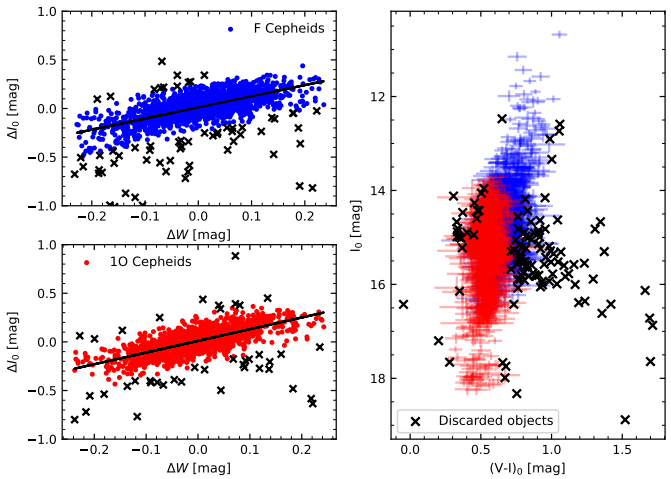

Fig. 3. Diagram of magnitude residuals of I-band P–L relation, ΔI_0, against the corresponding residuals of the P–W relation, ΔW, for F (upper left panel) and 1O (lower left panel) LMC Cepheids. Objects that deviate more than three sigma from this relation are marked with black crosses. These objects are also shown in a CMD of F (blue crosses) and 1O (red crosses) LMC Cepheids in the right panel.

the recent accurate determination by Pietrzyński et al. (2019). The distribution in the CMD of the final sample of 2058 F and 1387 1O Cepheids is shown in Fig. 4. Additionally, the position in the CMD of well-documented F and 1O Cepheids in eclipsing binaries, presented in Pilecki et al. (2018), was included.

3. Instability strip borders

The intrinsic width of the IS must be corrected for any effect that could change it, to be able to compare the strip with theoretical models. As we already removed all clear outliers (and those due to luminous companions) and objects with uncertain measurements from the sample, the major factor that is left is the effect of not perfectly known reddening. The nonzero uncertainties of the applied reddening values mean that the scatter of the Cepheid colors is higher and the IS width larger. The uncertainty of the

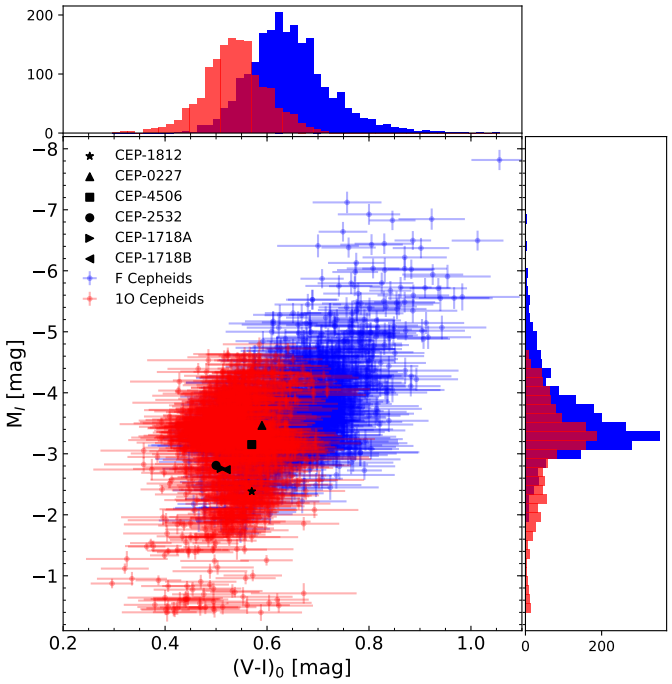

Fig. 4. CMD with I-band absolute magnitude for the final sample of F (blue) and 1O (red) LMC Cepheids. Data for well-documented Cepheids in eclipsing binaries are shown with different black symbols. Distributions of the intrinsic color $(V - I)_0$ and absolute magnitude M_I are shown in the upper and right subpanels, respectively.

photometry itself has a similar effect, but to a much lesser extent. We performed the following steps to obtain an intrinsic IS that is free of this effect. We binned the complete sample of F and 1O Cepheids (the one shown in Fig. 4) with respect to absolute magnitude in the I-band M_I. The central bins contain 233 stars, while the faintest and brightest bins contain around 100 stars. Firstly, we determined the initial blue and red edges of the IS of each bin by locating the 1st and 99th percentiles of the intrinsic color distribution, namely B_{1st} and R_{99th}, respectively. We then added random Gaussian errors to the intrinsic color of each Cepheid, making the distribution of color wider. Subsequently, we counted the number of extra stars that, after such procedure, are located outside the initial edges, that is, stars that are bluer or redder than B_{1st} or R_{99th}, respectively. We repeated this process 10 000 times and computed the median of the distribution of these numbers, namely n_{blue}, n_{red}.

The final blue and red IS positions of each bin, namely, B_{final} and R_{final}, were obtained by moving the initial edges "inside" the IS by n_{blue} and n_{red} stars, respectively. In this way, we subtract the widening effect due to reddening uncertainties and obtain a better approximation to the intrinsic IS. We note that only such corrected ISs can be compared directly with theoretical models that are not affected by reddening. The interior and exterior uncertainties in the intrinsic color of the IS were obtained by considering (instead of the median) the 16th and 84th percentiles of the distribution of the number of extra stars outside the initial edges, B_{1st} and R_{99th}. The positions in M_I of each bin of the IS edges were considered as the median of the M_I distribution of each bin. The computed IS boundaries, including F and 1O Cepheids, are shown in Fig. 5 as red circles. In this figure, the periods of the 1O Cepheids were fundamentalized using Eq. (1) of Pilecki et al. (2021). To obtain the overplotted constant period lines for one, three, and ten days we used the period-luminosity-color (PLC)

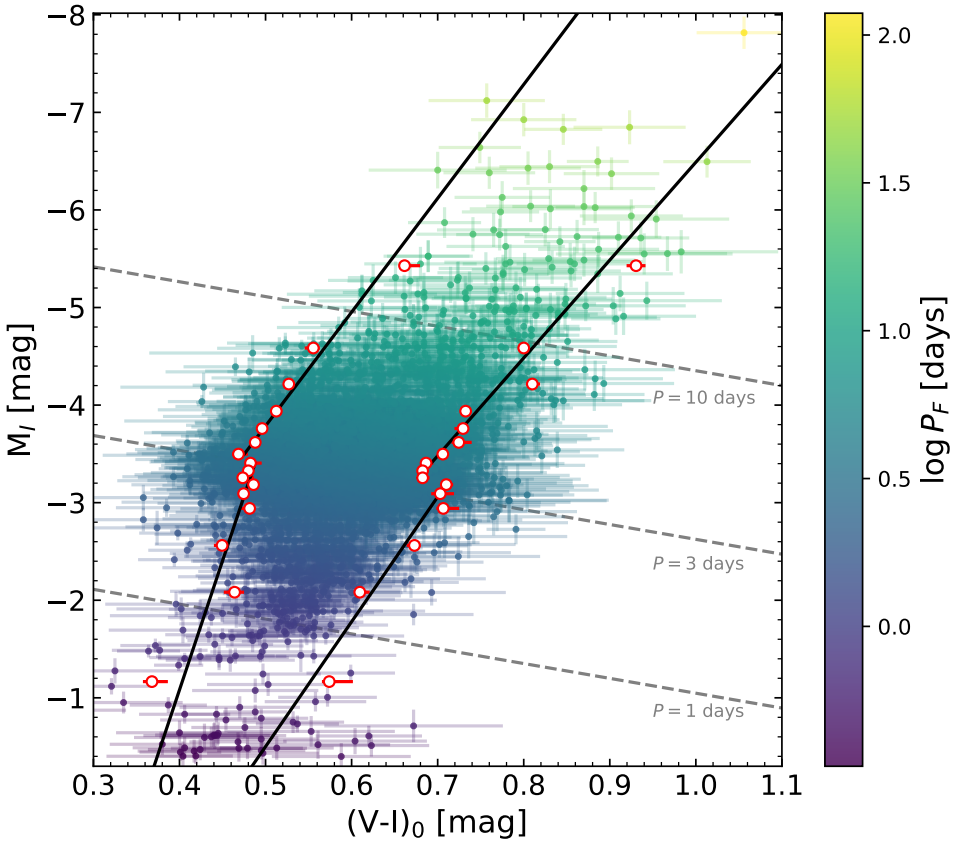

Fig. 5. CMD of F and 1O LMC Cepheids. The boundaries of our empirical IS are shown as red circles. Fits for the upper and lower part of the red and blue edges are shown as black solid lines. Periods for these stars are shown with a color gradient. For 1O Cepheids, periods were fundamentalized. Dashed lines of constant periods are overplotted. In most cases, error bars are smaller than the size of the points.

relation computed using the previously calculated I-band absolute magnitude and intrinsic color, and the periods provided in the OGLE catalog. Along the three-day constant period line, we notice a change of slope and discontinuity of the calculated edges between faint and bright Cepheids. A discussion of this phenomenon can be found in Sect. 4.1. Motivated by this detection, using the Python package `emcee` (Foreman-Mackey et al. 2013), we performed a linear fit with two parts for our empirical IS borders. In addition, a simplified wedge-shaped IS version was also computed. Coefficients of both formulations of the ISs are listed in Table 1. We repeated the IS edge determination process for F and 1O Cepheids separately, using bins that contain 162 and 109 stars, respectively. The obtained IS edges, for F and 1O Cepheids individually, are shown in Fig. 6 as red circles. We computed linear fits for fainter and brighter Cepheids and a wedge-shaped IS as in Fig. 5. The corresponding coefficients of the ISs can be found in Table 1.

Additionally, we determined the IS edges in a different way, to check the accuracy of the method presented above. In the other approach after adding random errors to the intrinsic color of the stars, we computed the 1st and 99th percentiles of the color distribution on each iteration, namely, $B^i_{1\mathrm{st}}$ and $R^i_{99\mathrm{th}}$, respectively. Afterward, we compared the mode of the distribution of $B^i_{1\mathrm{st}}$ and $R^i_{99\mathrm{th}}$ with the initial edges $B_{1\mathrm{st}}$ and $R_{99\mathrm{th}}$, calculating the respective differences (ΔB and ΔR). The initial edges were then corrected by ΔB and ΔR toward the IS interior. Both presented approaches yielded consistent results within errors. Nevertheless, the first presented method (correction by number) produced a smaller scatter of edge points and with smaller uncertainties.

As the reddening is one of the most important factors in a proper positioning of the IS edges, we did a check with two other previously mentioned reddening maps. The reddening map of the central regions of the LMC and SMC presented by Górski et al. (2020) was obtained using red clump stars selected from the data of OGLE-III, while similar maps of Chen et al. (2022) were derived from the SEDs of stellar sources using various large-scale surveys. We applied a reddening correction using their results and recomputed the IS edges of the sample including F and 1O Cepheids. The results were consistent with the ones obtained using the reddening map from Skowron et al. (2021; shown in Fig. 5). However, the blue edge obtained using the map of Górski et al. (2020) yielded a mean shift toward bluer colors of 0.07 mag, while the red edge obtained using the map of Chen et al. (2022) showed higher uncertainties.

4. Discussion

4.1. Break in IS boundaries in $(V - I)$ color

Independent from the used reddening maps, in all cases, a change in the slope and a discontinuity of the IS is observed over a period of three days, which makes this detection robust. We thus looked into possible explanations of this feature. Partially, it can be produced by the change of the fraction of F to 1O Cepheids at this period ($P \sim 3$ days, and $M_I \sim -3$), which can be seen in the histogram presented in Fig. 4. As the slopes for these modes differ (see Table 1), such a change makes the IS less steep above the break. Nevertheless, this break is also present in the IS edges of the F and 1O Cepheid subsamples (most noticeable in the red edge) presented in Fig. 6 and thus cannot be attributed only to the fraction change.

Previously in the literature, breaks in the P–L relation of F and 1O Cepheids have been reported in Magellanic Clouds. Bauer et al. (1999), Sharpee et al. (2002), and Sandage et al. (2009) found a slope change of the P–L relation for the SMC F Cepheids with periods shorter than two days. On the other hand, Sandage et al. (2004) and Ripepi et al. (2022) describe a break in the P–L relation for LMC Cepheids with periods of $P_{\mathrm{F}} = 10$ d

Table 1. Coefficients of the red and blue edges of the IS considering a break at $P = 3$ d, assuming $(V - I)_0 = \alpha(M_I + 3.5) + \beta$, for F and 1O mode together and separately.

P [d]	$\alpha_{\rm blue}$	$\beta_{\rm blue}$	$\sigma_{\alpha,\rm blue}$	$\sigma_{\beta,\rm blue}$	$\alpha_{\rm red}$	$\beta_{\rm red}$	$\sigma_{\alpha,\rm red}$	$\sigma_{\beta,\rm red}$
F and 1O Cepheids								
>3 d	−0.038	0.491	0.001	0.001	−0.078	0.734	0.003	0.004
>3 d	−0.086	0.475	0.002	0.001	−0.100	0.702	0.001	0.001
All	−0.059	0.490	0.0004	0.0002	−0.076	0.71	0.001	0.0004
F Cepheids								
>3 d	−0.046	0.553	0.007	0.003	−0.102	0.785	0.022	0.020
>3 d	−0.069	0.535	0.005	0.004	−0.118	0.712	0.003	0.002
All	−0.043	0.553	0.002	0.001	−0.089	0.727	0.001	0.001
1O Cepheids								
>3 d	−0.042	0.488	0.002	0.003	−0.025	0.643	0.003	0.004
>3 d	−0.065	0.466	0.006	0.004	−0.086	0.588	0.009	0.004
All	−0.038	0.482	0.001	0.001	−0.014	0.625	0.001	0.001

Notes. In addition, we include the coefficients for a fit without a break.

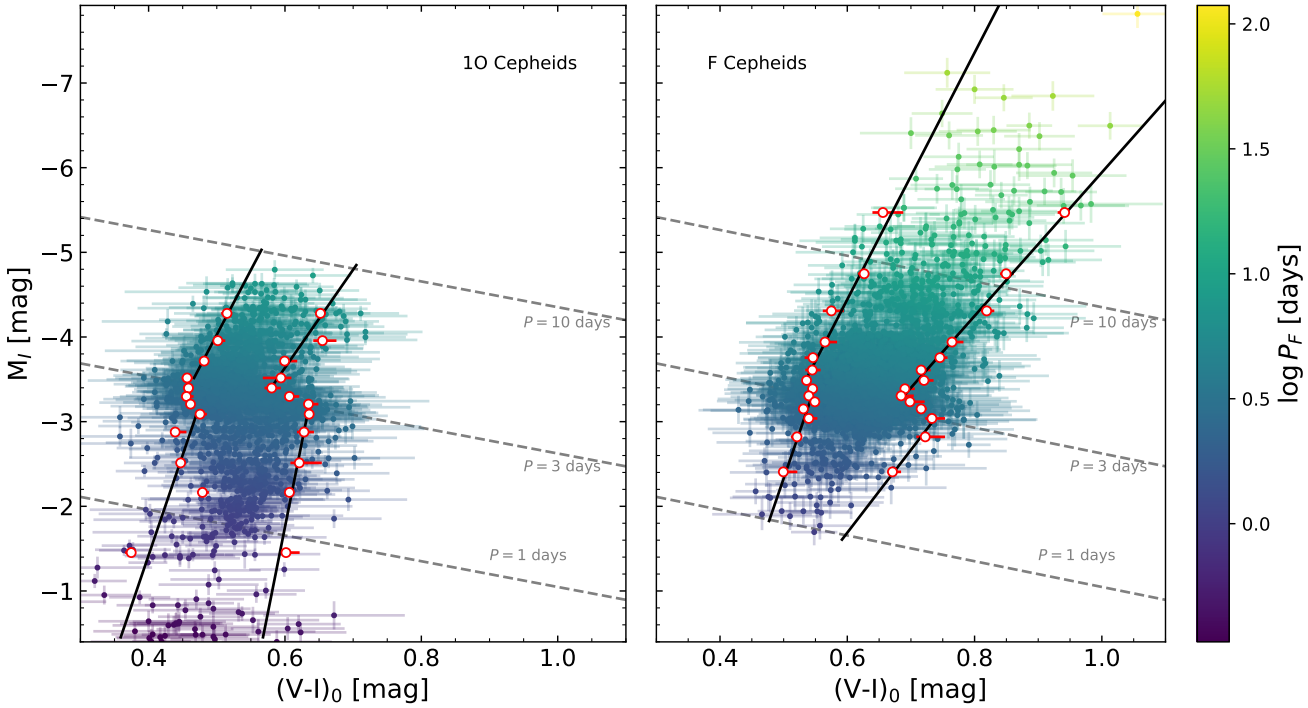

Fig. 6. Same as Fig. 5, but for 1O (left panel) and F (right panel) independently.

and $P_{\rm 1O} = 0.58$ d (the equivalent of $P_{\rm F} = 0.81$ d), respectively. Bhardwaj et al. (2016) performed an analysis of possible non-linearity in the P–L relations of Cepheids in the Magellanic Clouds, confirming the statistical significance of the aforementioned breaks.

Bauer et al. (1999) proposed several possible scenarios to explain the break of the P–L relation at two days for the SMC. One of these scenarios, also mentioned by Ripepi et al. (2022) with regard to the LMC, is the depopulation of second- and third-crossing Cepheids in the faint part of the IS due to the lower extension of the blue loops as the mass and period of Cepheids decrease. These stars spend less time inside the IS, or they do not enter it at all. This implies that Cepheids fainter than the break are likely on their first crossing of the IS. Such a scenario should be noticeable in the CMD and can have an impact on the shape of the IS.

In Fig. 7 we show an average P–L relation of our complete sample (considering F and 1O Cepheids); the periods of the 1O Cepheids were fundamentalized. In addition, a P–L relation with a break at $P = 3$ days is shown. Using the PLC relation we converted our IS to the period-luminosity plane and marked its edges with black triangles. In the right panel, we show residuals from the subtraction of the fit of the P–L relation with no break from the data. For periods shorter than $P \sim 3$ days, there is a sudden decrease in the number of Cepheids. Stars with periods shorter than 2.5 days or longer than about ten days tend to lay mostly below both P–L relations. The ten-day limit corresponds to the break reported in the literature, while below 0.81 days

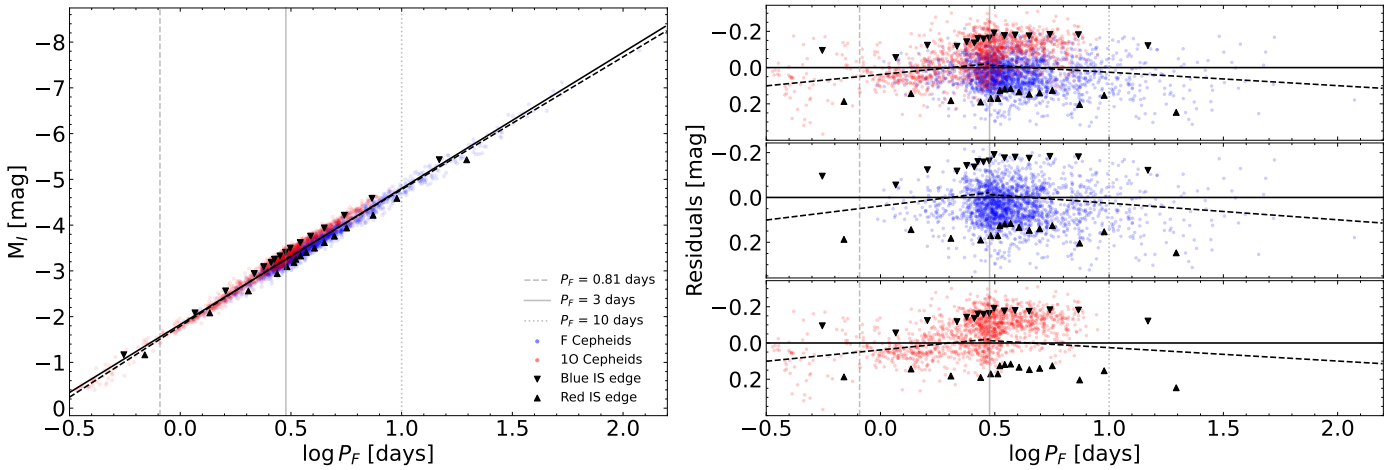

Fig. 7. P–L relation of F (blue points) and 1O (red points) LMC Cepheids (left panel). The 1O Cepheid periods were fundamentalized. The boundaries of the IS are displayed as black points. At $P_F = 0.81$, 3, and 10 days, a vertical gray line is traced. Average fits of the P–L relation considering the entire sample of stars and with a break at $P_F = 3$ days are shown as solid and dashed lines, respectively. The differences between the average fit of P–L with no break and the data are presented in the panels on the right, for the entire sample (upper), only F Cepheids (middle), and only 1O Cepheids (lower).

(a break from Ripepi et al. 2022) we can only see another significant decrease in the number of Cepheids. Regarding the IS edges, some change can be seen at these two period values, but the statistics are too low to quantify it reliably. We have to admit that because of the joint analysis of the F and 1O Cepheids the observations presented in this paragraph may slightly depend on the fundamentalization method used, but the results are consistent with what we can expect from the analysis of the color-magnitude diagram.

From a theoretical point of view, blue loops are very sensitive to metallicity and the adopted input physics, such as convective overshooting and nuclear reactions (Xu & Li 2004a,b; Walmswell et al. 2015). Several previous works in the literature have shown that the general trend for the blue loop extension is to decrease with stellar mass. In particular, for stars with $M < 4\,M_\odot$ the loops do not enter the IS at all (see, e.g., Anderson et al. 2016; De Somma et al. 2022). This supports the scenario of the depopulation of the faint part of the IS proposed by Bauer et al. (1999) and Ripepi et al. (2022).

To further test theoretical models and the depopulation scenario, we used the stellar evolution code Modules for Experiments in Stellar Astrophysics (MESA; Paxton et al. 2011, 2013, 2015, 2018, 2019; Jermyn et al. 2023) to calculate evolutionary tracks for nonrotating stars covering the mass range from 3 to 7 $M_\odot$ in steps of 0.1 $M_\odot$. We adopted $Z = 0.006$, 0.008, and 0.009 as representative metallicities for LMC stars (Romaniello et al. 2022). These tracks consider the solar mixture provided by Grevesse & Sauval (1998). We used a solar-calibrated mixing length parameter of $\alpha_{\rm mlt} = 1.9$. For the convective boundaries, we used the predictive mixing scheme described in Paxton et al. (2018), in addition to exponential core and envelope overshooting with the same parameter $f = 0.019$. The evolutionary tracks account for mass loss during the RGB, using the Reimers (1975) prescription, with a scaling factor $\eta_{\rm R} = 0.1$. The comparison between the evolutionary tracks and our empirical IS borders is shown in Fig. 8, where we show the extent of blue loops (presented as shaded areas) for each adopted metallicity. These areas are delimited by the position of the tip of the RGB on the red side and the hottest extreme of the blue loop on the blue side. The upper limits are artificial and are defined by the evolutionary tracks for 7 $M_\odot$-star with different metallicities. Evolutionary tracks with $M \lesssim 3.7$, 4.2, and 4.3 $M_\odot$ for $Z = 0.006$, 0.007, and 0.009, respectively, show blue loops that do not pass through the red edge of our IS. These limits and the corresponding limits in the CMD are in agreement with the break in our IS, and in favor of the scenario of the depopulation of the second- and third-crossing Cepheids at the faintest end of the Cepheid IS. As a consequence, in these mass ranges, we expect an increasingly (toward shorter P) large contribution of Cepheids at the first crossing through the IS, where they evolve on a short timescale of the H-shell burning phase. Such first-crossing Cepheids spend less time within the IS compared to higher mass Cepheids; thus, finding fewer stars in this part of the instability strip is expected. On the other hand, evolutionary tracks for masses larger than the above-mentioned limits present blue loops that cross the red edge of the IS, therefore the fraction of Cepheids in the second and third crossings, evolving on the longer timescale of the He-core burning phase, increases considerably. Since these stars spend more time inside the strip, their total number is much larger than the stars in the lower part of the IS. From the coincidence with the detected break we conclude that the evolutionary features mentioned above may be responsible for the shift of the faint IS edges to hotter temperatures and, partially, also for the change in the slopes (the latter being augmented by the change in the fraction of different modes).

4.2. Break in IS boundaries in $(V - K_s)$ color

Using the K_s-band data for Cepheids presented in Ripepi et al. (2022), we explored whether the break in the positions of the IS for the $V - I$ color index also appears for the $V - K_s$ index. We performed the same cleaning procedure mentioned in Sect. 2, obtaining a total sample of 3168 LMC Cepheids. After applying the method described in Sect. 3, we obtained empirical IS edges in the V and K_s bands. Figure 9 shows a CMD of the sample mentioned above and determined edges of the empirical IS as individual points and as a linear fit to these points considering a break. Due to the higher dependence of $V - K_s$ on temperature, the width of the IS in this color is larger than in the $V - I$, but the uncertainties (mostly due to the reddening) are significantly higher, which eventually leads to a lower relative precision of the $V - K_s$ data. As the $V - K_s$ sample is also slightly less numerous, we treat this analysis as auxiliary to that

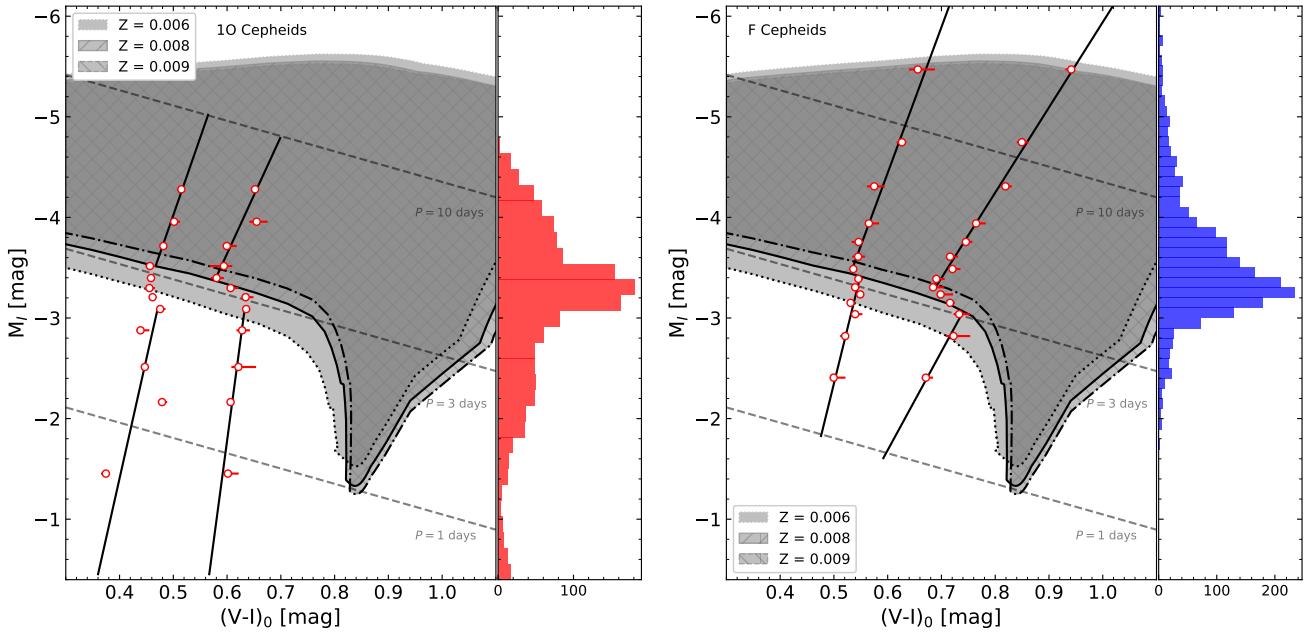

Fig. 8. CMD showing empirical IS limits (red points) separately for 1O (left panel) and F-mode (right panel) LMC Cepheids. Fits for the blue and red edges, considering a break at $P \sim 3$ days, are shown as solid lines. Gray shaded areas mark the blue loop extent (delimited by its bluest extreme and the tip of the RGB) for evolutionary tracks with masses from 3 to 7 $M_{\odot}$, and for $Z = 0.006$, 0.008, and 0.009. The upper limits for the areas are defined by the evolutionary tracks for 7 $M_{\odot}$ and would extend further up if tracks with higher masses are considered. The I-band absolute magnitude distributions of the 1O and F LMC Cepheids are shown on the right side of each panel.

of the $V - I$ data. Nevertheless, it is interesting to compare the results.

Similarly to the case with the V and I bands, the red border of the IS shows a clear change in the slope at $M_{K_s} \sim -4$, a value that corresponds to $P \sim 3$ days, approximately. Interestingly, contrary to the analysis with the $V-I$ color, with the $V-K_s$ index at the break there is no significant shift of the red edge toward redder colors for shorter period Cepheids. Analyzing the IS borders in the V and I bands, we identified two main factors responsible for the break: the change in the fraction of F to 1O Cepheids, and the depopulation of second- and third-crossing Cepheids in the lower part of the IS. The first factor applies to the $V - K_s$ color as well, as the edges for F Cepheids (analyzed separately) are less steep than for the 1O Cepheids also in these bands. The effect of the evolutionary factor is harder to evaluate. The use of the I band apparently enhances the difference between the Cepheids with periods shorter and longer than three days. However, if the I-band is for some reason more sensitive to the evolutionary stage (Hertzsprung gap vs. blue loop) than the K_s band, it would need another study. One also has to also note that both the wider IS and the higher uncertainties in $V - K$ may, to some extent, hinder the detection of discontinuity.

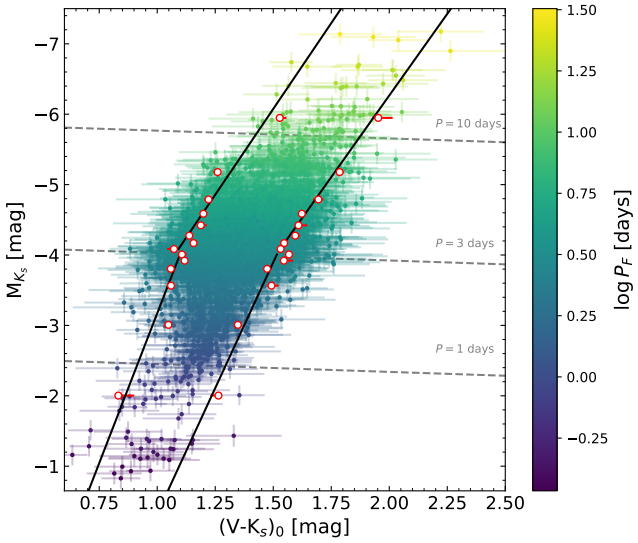

Fig. 9. Same as Fig. 5, but for V and K_s bands.

4.3. Comparison with LMC eclipsing binary stars

Graczyk et al. (2018) determined precise physical parameters of 20 eclipsing detached, double-lined LMC binary systems containing giant stars. Using the magnitudes in the I band, reddening, and third light provided in that work, we calculated the absolute magnitude in the I band and the intrinsic color $(V - I)_0$ for each component of the 20 systems. A CMD of the components of these systems, together with the two formulations (with and without a break) for the IS calculated in this work, is presented in Fig. 10. As expected, these stars lie outside our computed IS, since the components of these binary systems are G- and early K-type giant stars. Remarkably, one star of the systems, OGLE LMC-ECL-13360, is slightly outside the fitted lines of the red edge for our two versions of the IS within errors. Graczyk et al. (2018) showed that it is possible to fit both stars of this system with an isochrone without rotation. This fit indicates that the star closer to our IS is in the He-core burning phase, entering the IS, and would eventually start pulsating as a Cepheid.

4.4. Comparison with theoretical ISs

Previous works in the literature have obtained theoretical IS edges and have studied the effects of, for example, rotation,

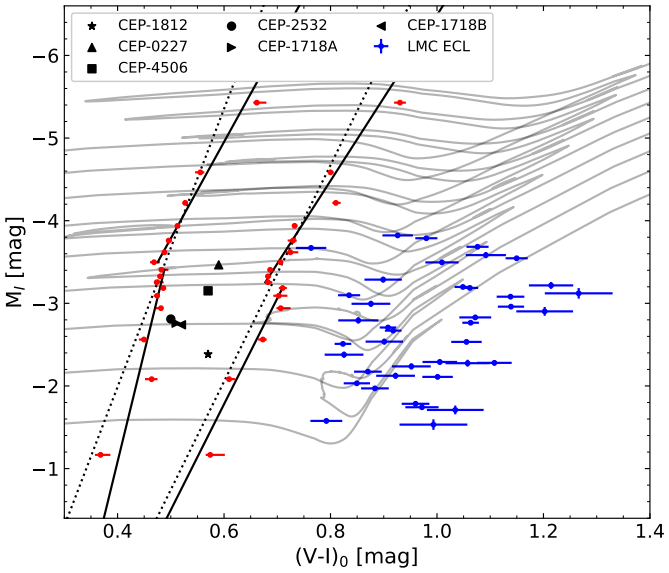

Fig. 10. CMD comparing our empirical IS (red points) with LMC eclipsing binary stars (black points). Data for well-documented Cepheids in eclipsing binaries are displayed as black symbols. Fits for the blue and red edges of the IS are shown as solid lines (considering a break) and dotted lines (without a break). In addition, evolutionary tracks of 3 to 7 $M_\odot$ in steps of 0.5 $M_\odot$ are presented as gray lines.

metallicity, and overshooting. By comparing these theoretical results with our empirical IS, it is possible to constrain some of the physical effects studied.

Each point of our IS for F Cepheids in the CMD plane was converted to the $\log T_{\rm eff} - \log L$ plane using the color-temperature and bolometric correction calibration presented by Worthey & Lee (2011). We averaged the effective temperature and luminosity calculated for each point, considering a surface gravity of $\log g = 1, 1.5, 2$, and 2.5. Then, the points were fit in the same way as for the IS in the color-magnitude diagram. The coefficients of the empirical instability strip in the $\log T_{\rm eff} - \log L$ plane are presented in Table 2. Since our empirical edges are composed of two parts, the conclusions may be different for the lower and upper parts of the IS. Additionally, our empirical results are based on a sample of Cepheids that have a nonzero spread in metallicity, which contributes to the uncertainty when comparing with theoretical models with a fixed metallicity.

In Fig. 11, we show the theoretical ISs for F Cepheids obtained by De Somma et al. (2022). Their models are based on Bag of Stellar Tracks and Isochrones (BaSTI; Hidalgo et al. 2018) evolutionary tracks that take into account instantaneous core overshooting with a free parameter equal to 0.2, mass loss with the Reimers formula considering $\eta = 0.3$, and a metallicity $Z = 0.008$. As far as their nonlinear pulsation calculations go, De Somma et al. (2022) approximated the effects of overshooting by considering an increase in the luminosity, over their canonical models (case A), of $\Delta(\log L/L_\odot) = 0.2$ dex (case B), and of $\Delta(\log L/L_\odot) = 0.4$ dex (case C), considering and additional three values for the superadiabatic convection efficiency, $\alpha_{ml} = 1.5$, $\alpha_{ml} = 1.7$, and $\alpha_{ml} = 1.9$. In the figure we show the linear and quadratic relations that describe the theoretical IS boundaries, provided by the authors. In the left panel, for clarity, we exclude their results for $\alpha_{ml} = 1.5$ given a weak agreement with our results. Globally, our empirical edges are most consistent with their models for case B and $\alpha_{ml} = 1.7$. However, there are some noticeable differences – their linear relations are systematically cooler than our upper blue edge, and their quadratic relations are systematically cooler than our lower blue edge. Moreover, even the edges that coincide better with the empirical ones have slightly different slopes.

The theoretical ISs for F Cepheids of Anderson et al. (2016) are shown in Fig. 12. They use the Geneva code of stellar evolution (Eggenberger et al. 2008), varying metallicity and the rate of rotation. We compared our results with their ISs for $Z = 0.006$ and three initial rotation rates, $\omega = 0.0$, 0.5, and 0.9. We reproduced their IS boundaries from Table A.2, where the effective temperature and luminosity of model stars entering or exiting the IS are given for each mass. For comparison with our empirical results, we used their results for the three crossings of the IS (if available) for all the provided masses. Their theoretical edges agree remarkably well with our empirical ones, both in regard to the zero points and the slopes, only with our lower blue edge being systematically cooler. One can note that their red edges present several shifts to higher temperatures. This is related to the dependency of the red IS boundary of the crossing number. After the first crossing, structural changes in the star affect the way convection operates. In addition, an increase in He content in the envelope occurs as a consequence of the first dredge-up. Both effects impact the position of the cool IS edge (Anderson et al. 2016). Globally their models with high rotation rates best describe our determined edges, but the lower part seems to favor those with moderate rotation rates.

Paxton et al. (2019) introduce Radial Stellar Pulsation RSP, a functionality in the MESA code to model high-amplitude, self-excited, nonlinear pulsations that the star develops when it crosses the IS. The RSP model depends on equations describing time-dependent convection from Kuhfuss (1986), implemented by Smolec & Moskalik (2008), which also depend on free parameters. Pulsation periods depend weakly on these parameters. However, period growth rates and light curves are sensitive to the choice of these convective variables. Different sets for these parameters are shown in Table 4 of Paxton et al. (2019). In Fig. 13, the theoretical ISs borders presented in Paxton et al. (2019, and priv. comm.) considering sets B and D for $Z = 0.008$ are shown. Their ISs were computed using second- and third-crossing Cepheid models. Set B of convective parameters adds radiative cooling effects to the convective model, while parameter set D simultaneously includes the effects of turbulent pressure and turbulent kinetic energy flux in addition to radiative cooling. As mentioned in Paxton et al. (2019), the IS edges produced by sets A and C overlap those for convective sets B and D, respectively. We can see that our blue edge is in closer agreement with that of set D, while our red edge lies somewhere in between sets B and D. The red edge is actually described better by set D for luminous long-period Cepheids, and by set B for short-period Cepheids if we extrapolate their red edge down to fainter Cepheids.

5. Conclusions

We used a sample of LMC Cepheids from the OGLE-IV catalog to compute the empirical, intrinsic instability strip. We determined the IS edges for F and 1O Cepheids, together and separately, using the I and V bands, and additionally using the V and K_s bands. In all cases, a break in the IS was observed at $\log P \sim 3$ days, which is most noticeable in the red edges and for separate 1O and F samples.

Using a set of evolutionary tracks computed with the stellar evolution code MESA, we investigated the scenario in which the origin of this break is explained by depopulation in the faint part

Table 2. Coefficients of the red and blue edges of the IS considering a break at $P = 3$ d, assuming $\log T_{\rm eff} = \alpha(\log L - 3.3) + \beta$, for F and 1O together and separately.

P [d]	$\alpha_{\rm blue}$	$\beta_{\rm blue}$	$\sigma_{\alpha,\rm blue}$	$\sigma_{\beta,\rm blue}$	$\alpha_{\rm red}$	$\beta_{\rm red}$	$\sigma_{\alpha,\rm red}$	$\sigma_{\beta,\rm red}$
F and 1O Cepheids								
<3 d	−0.021	3.805	0.001	0.0004	−0.057	3.732	0.002	0.002
>3 d	−0.058	3.800	0.001	0.0001	−0.074	3.737	0.001	0.0002
All	−0.035	3.802	0.0002	0.0001	−0.055	3.740	0.0004	0.0001
F Cepheids								
<3 d	−0.027	3.788	0.004	0.002	−0.045	3.732	0.008	0.004
>3 d	−0.048	3.788	0.004	0.001	−0.094	3.728	0.002	0.001
All	−0.032	3.787	0.001	0.0004	−0.072	3.729	0.0004	0.0002
1O Cepheids								
<3 d	−0.030	3.801	0.001	0.001	−0.017	3.768	0.003	0.002
>3 d	−0.038	3.807	0.004	0.0004	−0.062	3.774	0.007	0.001
All	−0.023	3.807	0.001	0.0002	−0.009	3.776	0.001	0.0002

Notes. In addition, we include the coefficients without break.

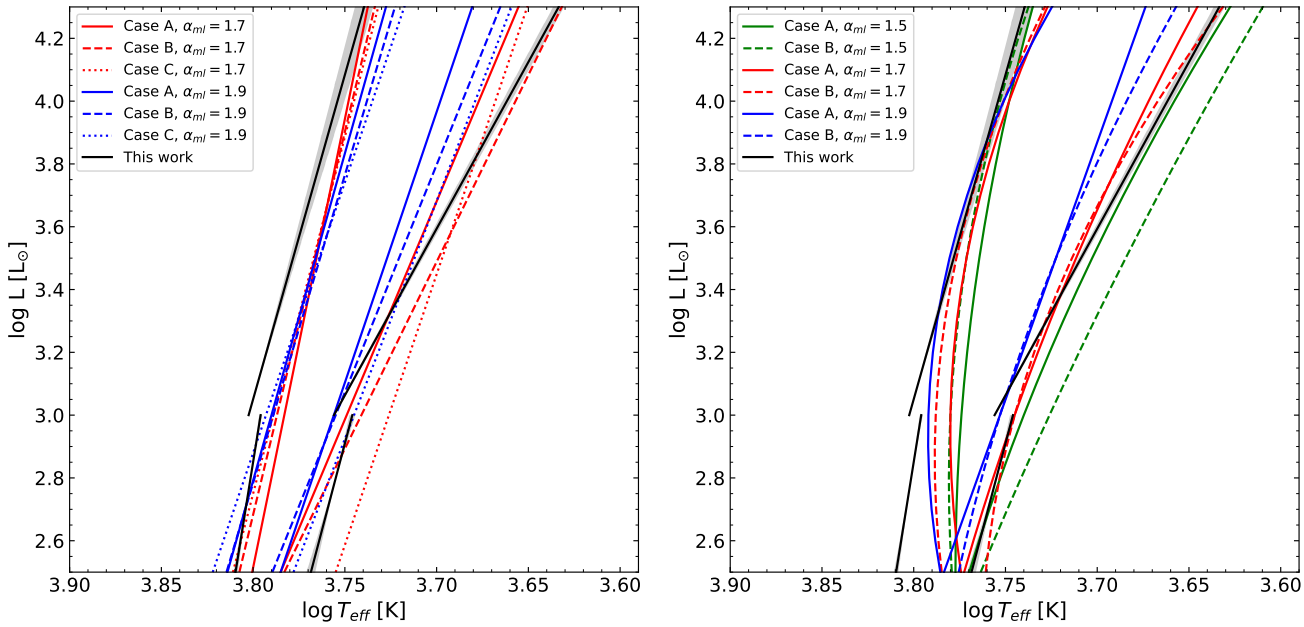

Fig. 11. Comparison of theoretical ISs considering linear (left panel) and quadratic (right panel) relations for $Z = 0.008$ presented in De Somma et al. (2022; red, blue, and green) and our empirical IS (black) in an HRD. Different line styles represent different cases of the luminosity adjustment (increase) applied by the authors to their canonical model. Different colors represent different efficiencies of superadiabatic convection α_{ml}. Shaded areas represent one sigma errors on the edges.

of the IS. Such depopulation would be caused by too low an extension of blue loops for lower mass stars, which would not evolve blueward enough to enter the instability strip. Our results confirmed the conclusions from other studies in the literature on that subject (Bauer et al. 1999; Ripepi et al. 2022).

Consequently, Cepheids with masses below ~4 $M_\odot$ would be found mostly during the first crossing of the IS, while above this limit there is a much higher contribution of Cepheids at the second and third crossings, for which the timescales are much longer. This change from the domination of the first to the domination of subsequent crossings coincides with the observed break in the IS edges and in the P–L relation. At the same time at different crossings, we may expect slightly different pulsational properties as the Cepheids are found at different evolutionary stages, namely the subgiant and blue loop phases of evolution (see Fig. 8). These two populations of Cepheids with different properties dominating at a given mass (or period) range, may then affect the position of the IS edges.

We compared our results with theoretical instability strips published in the literature. Our empirical edges are best described by the models of Anderson et al. (2016) with high rotation rates, for periods above the break, and by models with moderate rotation rates below the break. However, regarding the red edge only, models with $\omega = 0.9$ describe the whole range of pulsation periods well.

Regarding the instability strips that result from the models of De Somma et al. (2022) and Paxton et al. (2019), some fine-tuning of parameters would be needed to obtain consistent

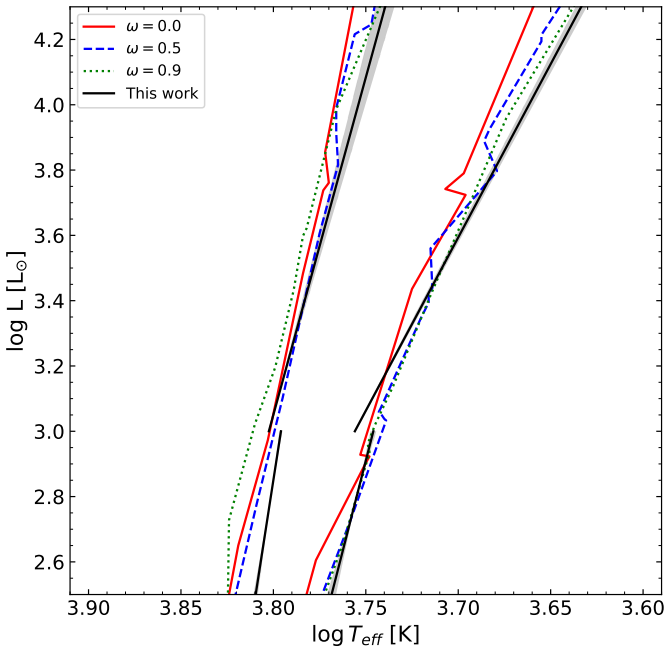

Fig. 12. Comparison of theoretical ISs for $Z = 0.006$ presented in Anderson et al. (2016; red, blue, and green) and our empirical IS (black) in an HRD. Different line styles represent different initial rotation rates ω, expressed as a fraction of critical velocity on ZAMS. Shaded areas represent one sigma errors on the edges.

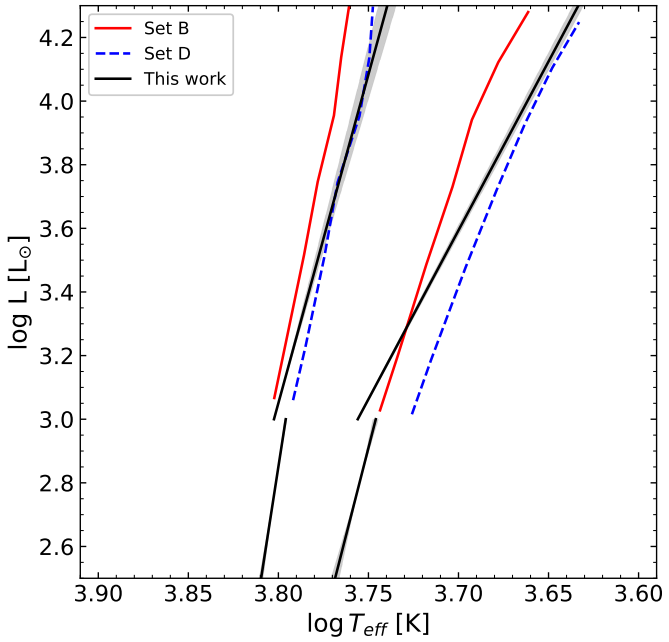

Fig. 13. Comparison of theoretical ISs for $Z = 0.008$ presented in Paxton et al. (2019; red and blue) and our empirical IS (black) in an HRD. Different line styles represent different sets of convective parameters of RSP. Shaded areas represent one sigma errors on the edges.

results. At the moment, no single set of their parameters produces an IS that would correspond well to our empirical edges – they either fall between the different sets or have different slopes.

Such fine-tuning is beyond the scope of this work but our empirical results may serve in the future to validate the theoretical models. Indeed, such a validation would be very welcome and useful to use the models for comparison with observations in environments in which the number of Cepheids is not high enough to empirically determine the IS edges. For example, such observationally calibrated models could serve to identify Cepheids in SN host galaxies. According to the comparison shown in this paper, models by Anderson et al. (2016) with either high rotation rates or a mixture of moderate and high rotation rates, depending on the pulsation period, currently provide the best agreement with the obtained empirical instability strip.

As the OGLE catalog of Cepheids in the LMC has a very high completeness level, we expect practically no improvement in the statistics in the future, except for the faintest Cepheids, perhaps. Nevertheless, in any future study, an improvement in the reddening determination and, to a lesser extent, photometric precision (mostly for faint stars) would help to obtain more accurate IS edges for the LMC galaxy. At the moment, however, the best way to achieve further insight into the physics of the instability strip is to study Cepheids in other galaxies. Not only does it provide a different and independent sample of stars, but it also lets us check on the effect of metallicity, which has a significant influence on the stellar evolution and pulsation. For that reason, our next step will be to perform a similar analysis for the SMC galaxy and compare the results.

Acknowledgements. We thank the anonymous referee for the constructive comments and suggestions. We acknowledge support from the Polish National Science Center grant SONATA BIS 2020/38/E/ST9/00486. R.S. is supported by the National Science Center, Poland, SONATA BIS project 2018/30/E/ST9/00598. This research has made use of NASA's Astrophysics Data System Service.

References

Anderson, R. I., Saio, H., Ekström, S., Georgy, C., & Meynet, G. 2016, A&A, 591, A8
Bauer, F., Afonso, C., Albert, J. N., et al. 1999, A&A, 348, 175
Bhardwaj, A., Kanbur, S. M., Macri, L. M., et al. 2016, MNRAS, 457, 1644
Bono, G., Caputo, F., Cassisi, S., et al. 2000a, ApJ, 543, 955
Bono, G., Castellani, V., & Marconi, M. 2000b, ApJ, 529, 293
Caldwell, J. A. R., & Laney, C. D. 1991, in The Magellanic Clouds, eds. R. Haynes, & D. Milne, 148, 249
Catelan, M., & Smith, H. A. 2015, Pulsating Stars (Weinheim: Wiley-VCH)
Chen, B. Q., Guo, H. L., Gao, J., et al. 2022, MNRAS, 511, 1317
De Somma, G., Marconi, M., Molinaro, R., et al. 2022, ApJS, 262, 25
Eggenberger, P., Meynet, G., Maeder, A., et al. 2008, Ap&SS, 316, 43
Fernie, J. D. 1990, ApJ, 354, 295
Fiorentino, G., Caputo, F., Marconi, M., & Musella, I. 2002, ApJ, 576, 402
Fiorentino, G., Marconi, M., Musella, I., & Caputo, F. 2007, A&A, 476, 863
Foreman-Mackey, D., Hogg, D. W., Lang, D., & Goodman, J. 2013, PASP, 125, 306
Górski, M., Zgirski, B., Pietrzyński, G., et al. 2020, ApJ, 889, 179
Graczyk, D., Pietrzyński, G., Thompson, I. B., et al. 2018, ApJ, 860, 1
Grevesse, N., & Sauval, A. J. 1998, Space Sci. Rev., 85, 161
Hidalgo, S. L., Pietrinferni, A., Cassisi, S., et al. 2018, ApJ, 856, 125
Houdek, G., & Dupret, M.-A. 2015, Liv. Rev. Sol. Phys., 12, 8
Inno, L., Bono, G., Matsunaga, N., et al. 2016, ApJ, 832, 176
Jacyszyn-Dobrzeniecka, A. M., Skowron, D. M., Mróz, P., et al. 2016, Acta Astron., 66, 149
Jermyn, A. S., Bauer, E. B., Schwab, J., et al. 2023, ApJS, 265, 15
Kuhfuss, R. 1986, A&A, 160, 116
Madore, B. F., Freedman, W. L., & Moak, S. 2017, ApJ, 842, 42
Martin, W. L., Warren, P. R., & Feast, M. W. 1979, MNRAS, 188, 139
Musella, I. 2022, Universe, 8, 335
Narloch, W., Pietrzyński, G., Kołaczkowski, Z., et al. 2019, MNRAS, 489, 3285
Paxton, B., Bildsten, L., Dotter, A., et al. 2011, ApJS, 192, 3
Paxton, B., Cantiello, M., Arras, P., et al. 2013, ApJS, 208, 4
Paxton, B., Marchant, P., Schwab, J., et al. 2015, ApJS, 220, 15
Paxton, B., Schwab, J., Bauer, E. B., et al. 2018, ApJS, 234, 34
Paxton, B., Smolec, R., Schwab, J., et al. 2019, ApJS, 243, 10
Pel, J. W., & Lub, J. 1978, in The HR Diagram – The 100th Anniversary of Henry Norris Russell, eds. A. G. D. Philip, & D. S. Hayes, 80, 229

Petroni, S., Bono, G., Marconi, M., & Stellingwerf, R. F. 2003, ApJ, 599, 522
Pietrzyński, G., Graczyk, D., Gallenne, A., et al. 2019, Nature, 567, 200
Pilecki, B. 2022, in XL Polish Astronomical Society Meeting, eds. E. Szuszkiewicz, A. Majczyna, K. Małek, et al., 12, 174
Pilecki, B., Gieren, W., Pietrzyński, G., et al. 2018, ApJ, 862, 43
Pilecki, B., Pietrzyński, G., Anderson, R. I., et al. 2021, ApJ, 910, 118
Pilecki, B., Thompson, I. B., Espinoza-Arancibia, F., et al. 2022, ApJ, 940, L48
Reimers, D. 1975, Mem. Soc. R. Sci. Liege, 8, 369
Ripepi, V., Chemin, L., Molinaro, R., et al. 2022, MNRAS, 512, 563
Romaniello, M., Riess, A., Mancino, S., et al. 2022, A&A, 658, A29
Sandage, A., Tammann, G. A., & Reindl, B. 2004, A&A, 424, 43
Sandage, A., Tammann, G. A., & Reindl, B. 2009, A&A, 493, 471
Schlegel, D. J., Finkbeiner, D. P., & Davis, M. 1998, ApJ, 500, 525
Sharpee, B., Stark, M., Pritzl, B., et al. 2002, AJ, 123, 3216
Skowron, D. M., Skowron, J., Udalski, A., et al. 2021, ApJS, 252, 23
Smolec, R., & Moskalik, P. 2008, Acta Astron., 58, 193
Soszyński, I., Udalski, A., Szymański, M. K., et al. 2017, Acta Astron., 67, 103
Tammann, G. A., Sandage, A., & Reindl, B. 2003, A&A, 404, 423
Turner, D. G. 2001, Odessa Astron. Publ., 14, 166
Ulaczyk, K., Szymański, M. K., Udalski, A., et al. 2013, Acta Astron., 63, 159
Walmswell, J. J., Tout, C. A., & Eldridge, J. J. 2015, MNRAS, 447, 2951
Worthey, G., & Lee, H. 2011, ApJS, 193, 1
Xu, H. Y., & Li, Y. 2004a, A&A, 418, 213
Xu, H. Y., & Li, Y. 2004b, A&A, 418, 225